

# MAGNETIC PROPERTIES AND MICROSTRUCTURE OF A BULK AMORPHOUS $\text{Fe}_{61}\text{Co}_{10}\text{Ti}_3\text{Y}_6\text{B}_{20}$ ALLOY, FABRICATED AS RODS AND TUBES

## MAGNETNE LASTNOSTI IN MIKROSTRUKTURA MASIVNE AMORFNE ZLITINE $\text{Fe}_{61}\text{Co}_{10}\text{Ti}_3\text{Y}_6\text{B}_{20}$ V OBLIKI PALIC IN CEVI

**Marcin Nabialek<sup>1</sup>, Katarzyna Bloch<sup>1</sup>, Karol Szlązak<sup>2</sup>, Michał Szota<sup>1</sup>**

<sup>1</sup>Czestochowa University of Technology, Institute of Physics, Faculty of Production Engineering and Materials Technology, 19 Armii Krajowej Av., 42-200 Czestochowa, Poland

<sup>2</sup>Warsaw University of Technology, Faculty of Materials Science and Engineering, 141 Woloska, 02-507 Warsaw, Poland  
23kasial@wp.pl

*Prejem rokopisa – received: 2014-07-31; sprejem za objavo – accepted for publication: 2015-03-10*

doi:10.17222/mit.2014.144

In this paper, studies are presented that characterize a bulk amorphous  $\text{Fe}_{61}\text{Co}_{10}\text{Ti}_3\text{Y}_6\text{B}_{20}$  alloy. Samples were fabricated in two forms: as a rod of 1 mm in diameter and as a tube of 1 mm in the outer diameter. The investigated material was obtained using the injection method, whereby the liquid alloy was injected into a copper mould. Using an X-ray diffractometer, a scanning electron microscope and computer tomography, the microstructures of these rapidly cooled samples were studied. Based on the obtained results, it was found that both the rod and the tube were fully amorphous. The cross-sections of the broken rod and tube were characterized by a mixed rupture consisting of smooth chevron and river patterns. This shows that there are regions of different ductility distributed throughout the volume of a sample. Three-dimensional images of the investigated materials, obtained with computer tomography, allowed the determination of the contribution of the pores (and their size) to the total volumes of the samples. The investigated alloy is a ferromagnetic material exhibiting good soft-magnetic properties such as a high saturation magnetization, a high magnetic permeability and a low value of the coercive field. The technique of injecting the liquid alloy into a copper mould, combined with the suction-casting method, can be used to produce toroidal cores that exhibit highly promising properties for a successful application in the construction of electric motors.

**Keywords:** bulk amorphous alloys, X-ray diffractometry, electron scanning microscopy, computer tomography, saturation magnetization, coercivity

Članek prikazuje študijo značilnosti masivne amorfne zlitine  $\text{Fe}_{61}\text{Co}_{10}\text{Ti}_3\text{Y}_6\text{B}_{20}$ , katere vzorci so bili izdelani na dva načina: kot palica premera 1 mm in kot cev z zunanjim premerom 1 mm. Preiskovani material je bil izdelan z vbrzgvanjem, saj je bila talina vbrzgvana v bakreno kokilo. Mikrostrukture hitro strjenih zlitin so bile proučevane s pomočjo rentgenskega difraktometra, z vrstičnim elektronskim mikroskopom in z računalniško tomografijo. Na podlagi dobljenih rezultatov je bilo ugotovljeno, da sta palica in cev popolnoma amorfni. Presek prelomljene palice in cevi ima mešan prelom, ki sestoji iz gladkih površin in stopnic v obliki rečic. To pomeni, da so različna področja duktilnosti razporejena po volumnu vzorca. Trodimenzionalne slike preiskovanih materialov, dobljenih s pomočjo računalniške tomografije, omogočajo določitev deleža por (in njihovih velikosti) v celotnem volumnu vzorcev. Preiskovana zlitina je feromagnetna in ima dobre mehko magnetne lastnosti, kot so: visoko nasičenje pri magnetizaciji, visoka magnetna permeabilnost in majhna vrednost koercitivnega polja. Tehniko vbrzgvanja tekoče litine v bakreno kokilo, v kombinaciji z livno metodo z vsesavanjem, se lahko uporabi za izdelavo toroidnih jeder, ki imajo dobre lastnosti za uspešno uporabo pri konstrukciji elektromotorjev.

**Ključne besede:** masivne amorfne zlitine, rentgenski difraktometer, vrstični elektronski mikroskop, računalniška tomografija, nasičena magnetizacija, koercitivnost

## 1 INTRODUCTION

The 21st century could be called the 'age of miniaturization and proliferation of the cutting-edge technology'. Currently, the rapid development of subassemblies for electronic devices is on the increase, featuring increasingly compact physical dimensions. Of particular importance are the component parts for miniature motors, targeted at specialist applications. The magnetic material used in micro-motors should have a good coefficient of fulfilment and, of course, excellent magnetic and mechanical properties.<sup>1-6</sup> Bulk amorphous alloys include highly promising materials for electrical-engineering applications.<sup>7-10</sup> Conventional amorphous alloys, manufactured in the form of a strip (ribbon), cannot be

used for the construction of micro-motors because the strip shape is not suitable for the application.

Through the selection of the right chemical composition for an alloy, the amorphous state can be obtained using a relatively slow cooling rate ( $10^2$  K/s –  $10^0$  K/s).<sup>11</sup> This feature has been utilized in the production of the so-called bulk amorphous alloys. The bulk amorphous alloys consist of many components (more than three chemical elements). In order to obtain a high value of the glass-forming ability (GFA) the atomic radii of the main alloy components must vary by more than 12 % and these components should be characterized by the negative mixing heat.<sup>11</sup> Moreover, the bulk amorphous alloys are characterized by a wide range of the so-called super-cooled liquid region,  $\Delta T_x (= T_x - T_g)$ , where  $T_x$  is

the crystallization-onset temperature and  $T_g$  is the glass-transition temperature.<sup>12</sup> Due to the facts that the bulk amorphous alloys consist of many components of various atomic radii and are obtained using a slow cooling rate, their density is higher than that typical of the classical amorphous alloys. The relatively slow cooling rate, used in the manufacture of the bulk amorphous alloys, yields a more relaxed structure in the resulting as-cast state.

This paper presents the results of the studies of the microstructure and magnetic properties of the  $\text{Fe}_{61}\text{Co}_{10}\text{Ti}_3\text{Y}_6\text{B}_{20}$  bulk amorphous alloy in the forms of a rod and a tube.

## 2 METHOD

The samples used in the investigations were produced of high-purity elements (greater than 99.95 % of amount fraction), using a combination of the injection- and suction-casting methods. The molten liquid was sucked into a water-cooled, copper die. The initial material was melted by arc melting (current range: 240–300 A; voltage: 80 V) under a protective atmosphere of inert gas. In addition, immediately prior to the suction process, pure titanium was re-melted in order to avoid a sample oxidation.

The structure and microstructure of the resulting material were investigated by means of an X-ray diffractometer (Bruker Advanced D8), scanning electron microscope (SEM – Zeiss, Supra 35) and computer tomograph (Bruker, SkyScan 1172 Micro-CT). X-ray diffraction patterns ( $\text{Cu-K}\alpha$ ) were taken in a 2-theta range from  $30^\circ$  to  $120^\circ$ , with a measurement step of  $0.05^\circ$  and time per step of 2 s. Images of the surfaces of the samples were obtained using the SEM, with a constant electron-acceleration voltage of 25 kV and the maximum magnification of  $12 \times 10^3$ . A three-dimensional visualization of the scanned samples was performed using the SkyScan software (Bruker). This kind of equipment is commonly used in amorphous and nanocrystalline materials investigations.<sup>13</sup> The X-ray parameters such as the voltage, the type of filter, the exposure time and the pixel size were optimized in order to obtain the best image contrast. The X-ray tube voltage was 100 kV and the current was 100  $\mu\text{A}$ . The X-ray

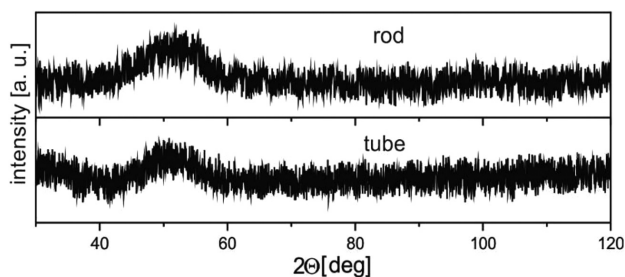


**Figure 1:** X-ray diffraction patterns for the  $\text{Fe}_{61}\text{Co}_{10}\text{Ti}_3\text{Y}_6\text{B}_{20}$  alloy  
**Slika 1:** Rentgenogram zlitine  $\text{Fe}_{61}\text{Co}_{10}\text{Ti}_3\text{Y}_6\text{B}_{20}$

projections were obtained at  $0.3^\circ$  intervals with a scanning angular rotation of  $360^\circ$  and 6 frames were averaged for each rotation. The obtained resolution yielded a pixel size of  $2.38 \mu\text{m}$ . In addition, ring artefacts were reduced through the selection of the random-movement amplitude of 50. The exposure time was 1200 ms. The images were reconstructed and analysed using the Bruker NRecon and CTAn software. DataViewer (Bruker) and CTVol (Bruker) were used to reveal the microstructural features of the samples. Static hysteresis loops were taken by means of a Lake Shore 7301 vibrating-sample magnetometer (VSM), using a magnetic field of up to 2 T.

## 3 RESULTS AND DISCUSSIONS

In **Figure 1**, X-ray diffraction patterns, obtained from the powdered alloy samples, are presented. A wide maximum, typical for the amorphous materials, can be observed on the X-ray diffraction patterns at  $2\Theta \approx 50^\circ$ . **Figure 2** shows SEM images of the investigated samples. Images showing the cross-sectional structures of the investigated samples are presented in **Figure 3**.

**Figure 3a** corresponds to the rod sample and reveals a visible mixed rupture, consisting of a smooth cleavage, a poorly developed chevron and river patterns. This is a sign of a varying degree of the structural relaxation of

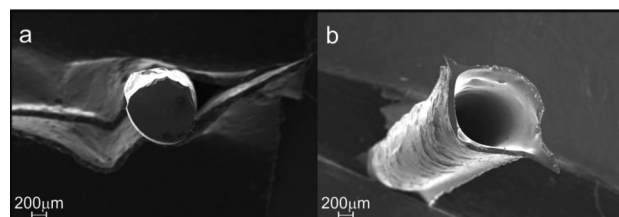


**Figure 2:** SEM images for the investigated samples: a) rod of a 1 mm diameter, b) tube of a 1 mm diameter

**Slika 2:** SEM-posnetka preiskovanih vzorcev: a) palica premera 1 mm, b) cev premera 1 mm

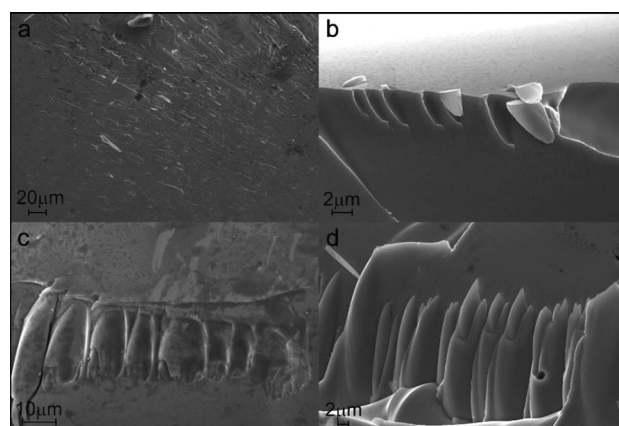


**Figure 3:** SEM images of the surfaces of the: a) rod and b), c), d) tube for the  $\text{Fe}_{61}\text{Co}_{10}\text{Ti}_3\text{Y}_6\text{B}_{20}$  alloy

**Slika 3:** SEM-posnetki površine palice: a) palica in b), c), d) cevka iz  $\text{Fe}_{61}\text{Co}_{10}\text{Ti}_3\text{Y}_6\text{B}_{20}$

the rod-shaped sample. Similar patterns were observed across the whole of the surface of the rod sample (**Figure 3a**). The cross-sectional images obtained for the tube-shaped sample (**Figures 3b to 3d**) were more inhomogeneous and different characters of the ruptures were observed for different sections of the tube. In **Figure 3b**, a well-developed band can be observed, dividing the regions of smooth and scale-like breakthroughs. At the top of this band, and situated perpendicularly to it, fine and poorly developed scales are visible. In another area of the investigated tube-like sample (**Figure 3c**), a band separating the regions of the smooth cleavage was also observed, with well-developed scales that are parallel to each other. In the lower part of the band determining the border of the scales, numerous breakthroughs appeared, indicating the direction of the created scale-like structure. In **Figure 3d**, the cross-section of the tube (with the parallel band of well-developed scales) can be seen. However, the character of this breakthrough is not typical. A further expansion of the scale-like structure is limited by the areas that feature different degrees of stress, and, as a result, double-graded scales can be observed.

On the basis of the SEM investigations, it can be stated that the quenching time (and, related with this, the cooling speed) has a significant influence on the structures of the breakthroughs featured in the investigated samples. The microstructures of the investigated rod- and tube-shaped samples are shown, with a 3-D visualisation, in **Figures 4 to 6**. On the basis of computed-tomography investigations of the rod-shaped sample of  $\text{Fe}_{61}\text{Co}_{10}\text{Ti}_3\text{Y}_6\text{B}_{20}$  alloy, it was found that its structure is uniform and free from defects in the form of pores; this is in agreement with the results of the SEM investigations (**Figure 3a**).

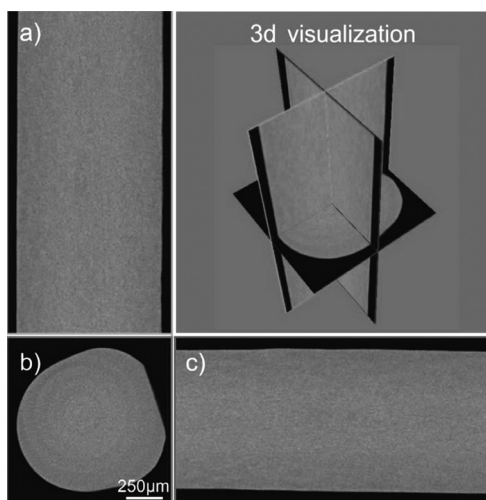


**Figure 4:** Three different cross-sectional views of the rod microstructure: a) coronal, b) transaxial, c) sagittal

**Slika 4:** Trije različni prikazi mikrostrukture preseka palice: a) koronalni, b) transaksialni, c) sagitalni

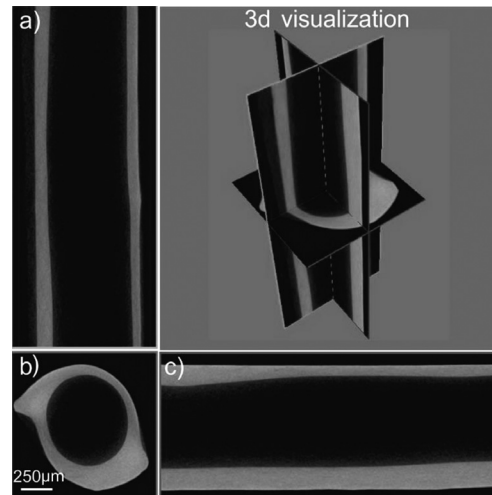


**Figure 5:** Three different cross-sectional views of the tube microstructure: a) coronal, b) transaxial, c) sagittal

**Slika 5:** Trije različni prikazi mikrostrukture preseka cevi: a) koronalni, b) transaksialni, c) sagitalni

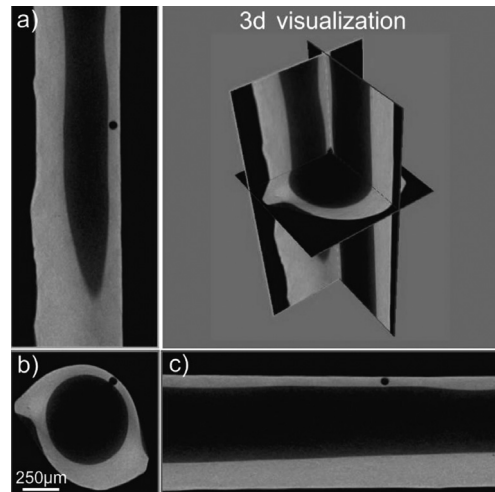


**Figure 6:** Three different cross-sectional views of the tube microstructure with open pores: a) coronal, b) transaxial, c) sagittal

**Slika 6:** Trije različni prikazi mikrostrukture preseka cevi z odprtimi porami: a) koronalni, b) transaksialni, c) sagitalni

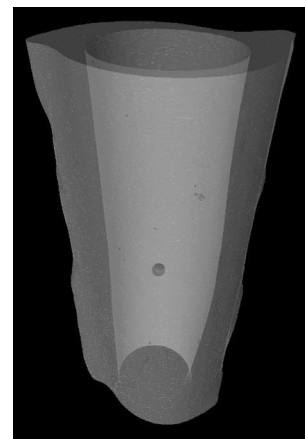


**Figure 7:** 3-D microstructure of the tube (in grey) with pores  
**Slika 7:** 3-D mikrostruktura cevi (siva barva) s porami

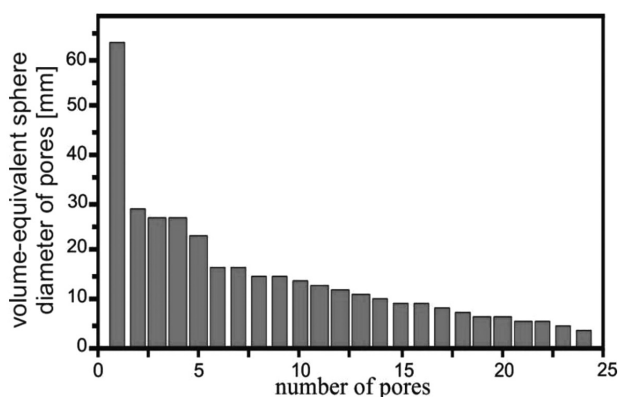


**Figure 8:** Volume-equivalent sphere diameter of the pores  
**Slika 8:** Volumenski ekvivalent kroglastega premera por

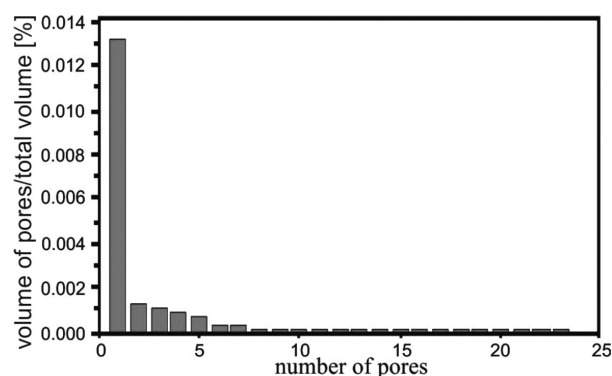


**Figure 9:** Ratio of the volume of the pores to the total volume  
**Slika 9:** Razmerje volumna por glede na celotni volumen

The microstructure of the tube was found to be mostly continuous (Figure 5) but there were some open and closed pores (Figure 6) that were visualized in 3-D (Figure 7). The volume-equivalent sphere diameter of the pores (Figure 8) revealed that there were only five pores of a volume of 0.0170 % in the range of 23  $\mu\text{m}$  – 63.7  $\mu\text{m}$  (Figure 9). The largest quantity of the pores (19) was in the range of 3.8  $\mu\text{m}$  to 17  $\mu\text{m}$ , but the volume was only 0.0014 % (Figure 9). In addition, various breakthrough structures, related with the varying thickness of the tube, can be observed in the SEM images (Figure 6).

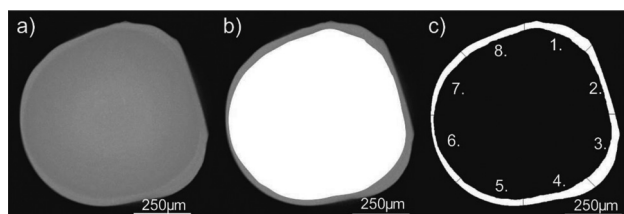


**Figure 10:** Microstructure of the rod: a) maximum intensity projection, b) differences for the main diameter (in white) and their distribution (in grey), c) thickness distribution divided into 8 parts  
**Slika 10:** Mikrostruktura palice: a) projekcija največje intenzivnosti, b) razlika med glavnim premerom (bela barva) in njihova razporeditev (siva barva), c) razporeditev debeline, razdeljene na 8 delov

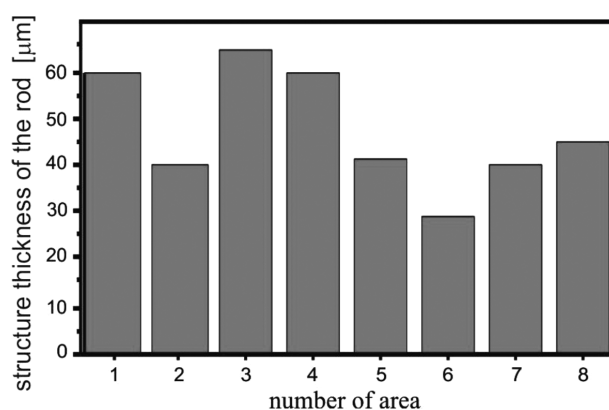


**Figure 11:** Rod thickness distribution divided into 8 parts (Figure 7c)  
**Slika 11:** Razporeditev debeline palice, razdeljene na 8 delov (Slika 7c)

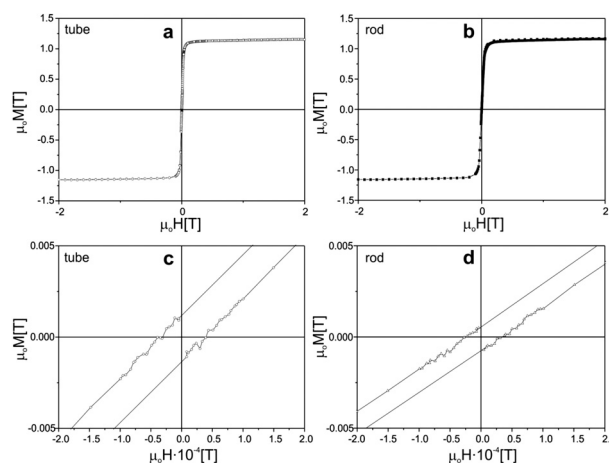


**Figure 12:** a), b) Static hysteresis loops, c), d) inserts with the origin of M-H system

**Slika 12:** a), b) Statične histerezne zanke ter c), d) vložki iz M-H sistema

The microstructure of the rod was continuous. To analyse the rod thickness, the distribution of maximum intensity projection (MIP) was used (Figure 10a). The differences, related to the main diameter (1082.2  $\mu\text{m}$ ), and their distribution are shown in Figure 10b. To calculate the thickness distribution of the rod, this area was divided into eight parts (Figure 10c) and analysed (Figure 11). The average shell thickness was found to be 47.4  $\mu\text{m}$ .

The measurements of the ‘magnetization versus magnetic field’ were performed on the rod- and tube-shaped samples of the  $\text{Fe}_{61}\text{Co}_{10}\text{Ti}_3\text{Y}_6\text{B}_{20}$  amorphous alloy (Figure 12). The static hysteresis loops were found to have the shapes typical for the ferromagnetic materials that exhibit soft-magnetic properties. The saturation-magnetization values for the rod- and tube-shaped samples of the investigated alloy were found to be almost identical, both being approximately 1.17 T. Moreover, the investigated alloys are characterized by low values of coercivity:  $0.37 \cdot 10^{-4}$  T and  $0.25 \cdot 10^{-4}$  T for the tube- and rod-shaped samples, respectively.

#### 4 CONCLUSIONS

The utilization of the combined injection-casting method, which features the suction casting of a molten alloy into a copper die, facilitated the fabrication of a bulk amorphous  $\text{Fe}_{61}\text{Co}_{10}\text{Ti}_3\text{Y}_6\text{B}_{20}$  alloy. In the case of the investigated alloy, the most important application parameters are the good soft-magnetic properties, attained whilst preserving the amorphous structure. Elements Ti and Y were used as the components facilitating the amorphicity of the alloy. It is commonly known that the addition of a small quantity of titanium (up to 5 % of amount fraction), or a similar addition of yttrium, to the Fe-based alloys improve their glass-forming ability (an increase in  $\Delta T_x$ ); however, usually this has a negative impact on the soft-magnetic properties. As demonstrated in this work, despite the addition of these components (3 % of amount fraction of Ti and 6 % of amount fraction of Y), the bulk amorphous  $\text{Fe}_{61}\text{Co}_{10}\text{Ti}_3\text{Y}_6\text{B}_{20}$  alloy is characterized by good soft-magnetic properties; i.e., a high value of the saturation magnetization (1.17 T) and low values of coercivity ( $0.37 \cdot 10^{-4}$  T and  $0.25 \cdot 10^{-4}$  T for the tube and rod samples, respectively).

When carrying out a computer-tomography investigation of the rod-shaped sample of the  $\text{Fe}_{61}\text{Co}_{10}\text{Ti}_3\text{Y}_6\text{B}_{20}$  alloy, no pores were observed in the structure. However, during the production of the tube-shaped sample, pores were found in the volume of the sample. The volume-equivalent sphere diameter of the pores indicated that there were only five pores within a range of 23–63.7  $\mu\text{m}$  with a volume of 0.0170 %. The largest quantity of the pores was within a range of 3.8  $\mu\text{m}$  to 17  $\mu\text{m}$ , but their volume comprised only 0.0014 %. The presence of the pores within the volume of the tube-shaped sample caused only a minor deterioration of the magnetic properties in comparison with the rod-shaped sample (an increase in the coercivity). Despite this, the material can be used for the magnetic cores in micromotors, for applications involving miniature devices.

By regulating the technical parameters of the production process, it was possible for the rod- or tube-shaped samples to be obtained. On the basis of the performed investigations, it can be stated that a variation in the quenching speed of the molten alloy has a substantial influence on the structure, the microstructure and some of the magnetic properties of the investigated material. Hitherto, the bulk amorphous alloys have been produced mainly in the forms of rods and plates. The creation of bulk samples in the form of closed rings is a major technological step. During the production process, an additional problem was the appearance of the pores in the volume of the tube, which had deleterious effects on the durability and soft-magnetic properties of the investigated alloy. Given an appropriate chemical composition, these rings could be used in the construction of the magnetic cores in electronic and electric microdevices.

The results of the investigations presented in this paper demonstrate that changes in the structural stresses and quenching speed of the molten alloy have a major

influence on the value of the coercivity, which is a measure of the energy required for demagnetizing the material. Despite a minor increase in the value of the coercivity for the tube-shaped sample, the material formed in this shape can be used for the magnetic cores of micromotors in miniaturized devices.

#### 5 REFERENCES

- A. Inoue, Bulk amorphous alloys with soft and hard magnetic properties, *Materials Science and Engineering*, 226–228 (1997), 357–363, doi:10.1016/S0921-5093(97)80049-4
- M. Nabialek, J. Zbrozarczyk, J. Olszewski, M. Hasiak, W. Cieurzyńska, K. Sobczyk, J. Świerczek, J. Kaleta, A. Łukiewska, Microstructure and magnetic properties of bulk amorphous and nanocrystalline  $\text{Fe}_{61}\text{Co}_{10}\text{Zr}_{2.5}\text{Hf}_{2.5}\text{Nb}_2\text{W}_2\text{B}_{20}$  alloy, *Journal of Magnetism and Magnetic Materials*, 320 (2008), 787–791, doi:10.1016/j.jmmm.2008.04.046
- T. Kozieł, J. Latuch, S. Kąc, Structure of melt-spun Fe–Cu–Si–B–Nb alloy, *Journal of Alloys and Compounds*, 586 (2014) S121–S125, doi:10.1016/j.jallcom.2012.11.169
- J. Gondro, J. Świerczek, J. Olszewski, J. Zbrozarczyk, K. Sobczyk, W. Cieurzyńska, J. Rzącki, M. Nabialek, Microstructure and some magnetic properties of bulk amorphous  $(\text{Fe}_{0.61}\text{Co}_{0.10}\text{Zr}_{0.025}\text{Hf}_{0.025}\text{Ti}_{0.02}\text{W}_{0.02}\text{B}_{0.20})_{100-x}\text{Y}_x$  ( $x = 0, 2, 3$  or  $4$ ) alloys, *Journal of Magnetism and Magnetic Materials*, 324 (2012), 1360–1364, doi:10.1016/j.jmmm.2011.11.038
- R. Hasegawa, Soft magnetic properties of metallic glasses, *Journal of Magnetism and Magnetic Materials*, 41 (1984), 79–85, doi:10.1016/0304-8853(84)90142-2
- H. Jian, W. Luo, S. Tao, M. Yan, Mechanical and magnetic properties of  $(\text{Fe}_{72}\text{Mo}_4\text{B}_{24})_{100-x}\text{Tb}_x$  ( $x = 4, 5, 6, 7$  at.%) bulk glassy alloys, *Journal of Alloys and Compounds*, 505 (2010), 315–318, doi:10.1016/j.jallcom.2010.06.061
- T. Kozieł, J. Latuch, A. Zielińska-Lipiec, Structure of the amorphous-crystalline  $\text{Fe}_{66}\text{Cu}_6\text{B}_{19}\text{Si}_5\text{Nb}_4$  alloy obtained by the melt-spinning process, *Archives of Metallurgy and Materials*, 58 (2013) 601–605, doi: 10.2478/amm-2013-0044
- M. Hasiak, K. Sobczyk, J. Zbrozarczyk, W. Cieurzyńska, J. Olszewski, M. Nabialek, J. Kaleta, J. Świerczek, A. Łukiewska, Some Magnetic Properties of Bulk Amorphous Fe–Co–Zr–Hf–Ti–W–B–(Y) Alloys, *IEEE Transactions on Magnetics*, 44 (2008), 3879–3882, doi:10.1109/TMAG.2008.2002248
- K. Błoch, J. Gondro, P. Pietrusiewicz, M. Dośpiał, M. Nabialek, M. Szota, K. Gruszka, Time and thermal stability of magnetic properties in  $\text{Fe}_{61}\text{Co}_{10}\text{Y}_8\text{Nb}_1\text{B}_{20}$  bulk amorphous alloys, *Acta Physica Polonica A*, 126 (2014), 108–109, doi:10.12693/APhysPolA.126.108
- H. Chirac, N. Lupu, Design and preparation of new soft magnetic bulk amorphous alloys for applications, *Materials Science and Engineering A*, 375–377 (2004), 255–259, doi:10.1016/j.msea.2003.10.007
- K. Sobczyk, J. Świerczek, J. Gondro, J. Zbrozarczyk, W. Cieurzyńska, J. Olszewski, P. Brągiel, A. Łukiewska, J. Rzącki, M. Nabialek, Microstructure and some magnetic properties of bulk amorphous  $(\text{Fe}_{0.61}\text{Co}_{0.10}\text{Zr}_{0.025}\text{Hf}_{0.025}\text{Ti}_{0.02}\text{W}_{0.02}\text{B}_{0.20})_{100-x}\text{Y}_x$  ( $x=0, 2, 3$  or  $4$ ) alloys, *Journal of Magnetism and Magnetic Materials*, 324 (2012), 540–549, doi:10.1016/j.jmmm.2011.08.038
- A. Inoue, W. Zhang, T. Zhang, K. Kurosaka, High-strength Cu-based bulk glassy alloys in Cu–Zr–Ti and Cu–Hf–Ti ternary systems, *Acta Materialia*, 49 (2001), 2645–2652, doi:10.1016/S1359-6454(01)00181-1
- K. Gruszka, M. Nabialek, K. Błoch, S. Walters, Analysis of the structure (XRD) and microstructure (TEM, SEM, AFM) of bulk amorphous and nanocrystalline alloys based on FeCoB, *International Journal of Materials Research*, 106 (2015) 7, 689–696, doi: 10.3139/146.111226